1-1-2006

Search for the Θ+ pentaquark in the reactions γp→K⁻⁻⁻0K+n and γp→K⁻⁻⁻0K0p

R. DeVita

Angela Biselli
Fairfield University, abiselli@fairfield.edu

CLAS Collaboration

Peer Reviewed

Published Citation

R. De Vita et al. [CLAS Collaboration], "Search for the Θ+ pentaquark in the reactions γp→K⁻⁻⁻0K+n and γp→K⁻⁻⁻0K0p", Physical Review D 74.3 (2006) DOI: 10.1103/PhysRevD.74.032001

Search for the Θ^+ pentaquark in the reactions $\gamma p \to \bar{K}^0 K^+ n$ and $\gamma p \to \bar{K}^0 K^0 p$

R. De Vita,[1] M. Battaglieri,[1] V. Kubarovsky,[2] N. A. Baltzell,[3] M. Bellis,[2,4] J. Goett,[2] L. Guo,[5] G. S. Mutchler,[6] P. Stoler,[2] M. Ungaro,[2,7] D. P. Weygand,[5] M. J. Amaryan,[34] P. Ambrozewicz,[17] M. Anghinolfi,[1] G. Asryan,[40] H. Avakian,[5] H. Bagdasaryan,[34] N. Baillie,[39] J. P. Ball,[9] V. Batourine,[28] I. Bedlinskiy,[25] N. Benmouna,[19] B. L. Berman,[19] A. S. Biselli,[4,16] S. Boiarinov,[5] S. Bouchigny,[23] R. Bradford,[4] D. Branford,[15] W. J. Briscoe,[19] W. K. Brooks,[5] S. Bültmann,[34] V. D. Burkert,[5] C. Butuceanu,[39] J. R. Calarco,[31] S. L. Careccia,[34] D. S. Carman,[33] S. Chen,[18] E. Clinton,[29] P. L. Cole,[21] P. Collins,[9] P. Coltharp,[18] D. Crabb,[38] H. Crannell,[12] V. Crede,[18] J. P. Cummings,[2] D. Dale,[41] R. De Masi,[13] E. De Sanctis,[22] P. V. Degtyarenko,[5] A. Deur,[5] K. V. Dharmawardane,[34] C. Djalali,[3] G. E. Dodge,[34] J. Donnelly,[20] D. Doughty,[5,14] M. Dugger,[9] O. P. Dzyubak,[3] H. Egiyan,[5,*] K. S. Egiyan,[40] L. El Fassi,[8] L. Elouadrhiri,[5] P. Eugenio,[18] G. Fedotov,[30] H. Funsten,[39] M. Y. Gabrielyan,[41] L. Gan,[42] M. Garçon,[13] A. Gasparian,[43] G. Gavalian,[31,34] G. P. Gilfoyle,[35] K. L. Giovanetti,[26] F. X. Girod,[13] O. Glamazdin,[27] J. T. Goetz,[10] E. Golovach,[30] A. Gonenc,[17] C. I. O. Gordon,[20] R. W. Gothe,[3] K. A. Griffioen,[39] M. Guidal,[23] N. Guler,[34] V. Gyurjyan,[5] C. Hadjidakis,[23] K. Hafidi,[8] H. Hakobyan,[40] R. S. Hakobyan,[12] J. Hardie,[5,14] F. W. Hersman,[31] K. Hicks,[33] I. Hleiqawi,[33] M. Holtrop,[31] C. E. Hyde-Wright,[34] Y. Ilieva,[19] D. G. Ireland,[20] B. S. Ishkhanov,[30] E. L. Isupov,[30] M. M. Ito,[5] D. Jenkins,[37] H. S. Jo,[23] K. Joo,[7] H. G. Juengst,[19,†] J. D. Kellie,[20] M. Khandaker,[32] W. Kim,[28] A. Klein,[34] F. J. Klein,[12] A. V. Klimenko,[34] M. Kossov,[25] L. H. Kramer,[5,17] J. Kuhn,[4] S. E. Kuhn,[34] S. V. Kuleshov,[25] J. Lachniet,[4,†] J. M. Laget,[5,13] J. Langheinrich,[3] D. Lawrence,[29] T. Lee,[31] Ji Li,[2] K. Livingston,[20] H. Y. Lu,[3] M. MacCormick,[23] N. Markov,[7] B. McKinnon,[20] B. A. Mecking,[5] J. J. Melone,[20] M. D. Mestayer,[5] C. A. Meyer,[4] T. Mibe,[33] K. Mikhailov,[25] R. Minehart,[38] M. Mirazita,[22] R. Miskimen,[29] V. Mochalov,[24] V. Mokeev,[30] L. Morand,[13] S. A. Morrow,[13,23] M. Moteabbed,[17] P. Nadel-Turonski,[19] I. Nakagawa,[44] R. Nasseripour,[3,17] S. Niccolai,[23] G. Niculescu,[26] I. Niculescu,[26] B. B. Niczyporuk,[5] M. R. Niroula,[34] R. A. Niyazov,[5] M. Nozar,[5] M. Osipenko,[1,30] A. I. Ostrovidov,[18] K. Park,[28] E. Pasyuk,[9] C. Paterson,[20] J. Pierce,[38] N. Pivnyuk,[25] D. Pocanic,[38] O. Pogorelko,[25] S. Pozdniakov,[25] J. W. Price,[10,11] Y. Prok,[38,‡] D. Protopopescu,[20] B. A. Raue,[5,17] G. Riccardi,[18] G. Ricco,[1] M. Ripani,[1] B. G. Ritchie,[9] F. Ronchetti,[22] G. Rosner,[20] P. Rossi,[22] F. Sabatié,[13] C. Salgado,[32] J. P. Santoro,[5,12] V. Sapunenko,[5] R. A. Schumacher,[4] V. S. Serov,[25] Y. G. Sharabian,[5] N. V. Shvedunov,[30] E. S. Smith,[5] L. C. Smith,[38] D. I. Sober,[12] A. Stavinsky,[25] S. S. Stepanyan,[28] S. Stepanyan,[5] B. E. Stokes,[18] I. I. Strakovsky,[19] S. Strauch,[19,§] M. Taiuti,[1] D. J. Tedeschi,[3] A. Teymurazyan,[41] U. Thoma,[5,‖] A. Tkabladze,[19] S. Tkachenko,[34] L. Todor,[35] C. Tur,[3] M. F. Vineyard,[36] A. V. Vlassov,[25] D. P. Watts,[20,¶] L. B. Weinstein,[34] M. Williams,[4] E. Wolin,[5] M. H. Wood,[3,**] A. Yegneswaran,[5] L. Zana,[31] J. Zhang,[34] B. Zhao,[7] and Z. Zhao[3]

(CLAS Collaboration)

[1]*Istituto Nazionale di Fisica Nucleare, Sezione di Genova, and Dipartimento di Fisica, Università di Genova, 16146 Genova, Italy*
[2]*Rensselaer Polytechnic Institute, Troy, New York 12180-3590, USA*
[3]*University of South Carolina, Columbia, South Carolina 29208, USA*
[4]*Carnegie Mellon University, Pittsburgh, Pennsylvania 15213, USA*
[5]*Thomas Jefferson National Accelerator Facility, Newport News, Virginia 23606, USA*
[6]*Rice University, Houston, Texas 77005-1892, USA*
[7]*University of Connecticut, Storrs, Connecticut 06269, USA*
[8]*Argonne National Laboratory*
[9]*Arizona State University, Tempe, Arizona 85287-1504, USA*
[10]*University of California at Los Angeles, Los Angeles, California 90095-1547, USA*
[11]*California State University, Dominguez Hills, California 90747-0005, USA*
[12]*Catholic University of America, Washington, D.C. 20064, USA*
[13]*CEA-Saclay, Service de Physique Nucléaire, F91191 Gif-sur-Yvette, France*
[14]*Christopher Newport University, Newport News, Virginia 23606, USA*
[15]*Edinburgh University, Edinburgh EH9 3JZ, United Kingdom*
[16]*Fairfield University, Fairfield Connecticut 06824, USA*
[17]*Florida International University, Miami, Florida 33199, USA*
[18]*Florida State University, Tallahassee, Florida 32306, USA*
[19]*The George Washington University, Washington, D.C. 20052, USA*
[20]*University of Glasgow, Glasgow G12 8QQ, United Kingdom*
[21]*Idaho State University, Pocatello, Idaho 83209, USA*
[22]*INFN, Laboratori Nazionali di Frascati, 00044 Frascati, Italy*
[23]*Institut de Physique Nucleaire ORSAY, Orsay, France*

[24]*Institute for High Energy Physics, Protvino, 142281, Russia*
[25]*Institute of Theoretical and Experimental Physics, Moscow, 117259, Russia*
[26]*James Madison University, Harrisonburg, Virginia 22807, USA*
[27]*Kharkov Institute of Physics and Technology, Kharkov 61108, Ukraine*
[28]*Kyungpook National University, Daegu 702-701, South Korea*
[29]*University of Massachusetts, Amherst, Massachusetts 01003, USA*
[30]*General Nuclear Physics Institute, Moscow State University, 119899 Moscow, Russia*
[31]*University of New Hampshire, Durham, New Hampshire 03824-3568, USA*
[32]*Norfolk State University, Norfolk, Virginia 23504, USA*
[33]*Ohio University, Athens, Ohio 45701, USA*
[34]*Old Dominion University, Norfolk, Virginia 23529, USA*
[35]*University of Richmond, Richmond, Virginia 23173, USA*
[36]*Union College, Schenectady, New York 12308, USA*
[37]*Virginia Polytechnic Institute and State University, Blacksburg, Virginia 24061-0435, USA*
[38]*University of Virginia, Charlottesville, Virginia 22901, USA*
[39]*College of William and Mary, Williamsburg, Virginia 23187-8795, USA*
[40]*Yerevan Physics Institute, 375036 Yerevan, Armenia*
[41]*University of Kentucky, Lexington, Kentucky 40506, USA*
[42]*University of North Carolina, Wilmington, North Carolina 28403, USA*
[43]*North Carolina Agricultural and Technical State University, Greensboro, North Carolina 27455, USA*
[44]*The Institute of Physical and Chemical Research, RIKEN, Wako, Saitama 351-0198, Japan*
(Received 27 June 2006; published 1 August 2006)

The exclusive reactions $\gamma p \to \bar{K}^0 K^+ n$ and $\gamma p \to \bar{K}^0 K^0 p$ have been studied in the photon energy range 1.6–3.8 GeV, searching for evidence of the exotic baryon $\Theta^+(1540)$ in the decays $\Theta^+ \to nK^+$ and $\Theta^+ \to pK^0$. Data were collected with the CLAS detector at the Thomas Jefferson National Accelerator Facility. The integrated luminosity was about 70 pb^{-1}. The reactions have been isolated by detecting the K^+ and proton directly, the neutral kaon via its decay to $K_S \to \pi^+\pi^-$ and the neutron or neutral kaon via the missing mass technique. The mass and width of known hyperons such as Σ^+, Σ^- and $\Lambda(1116)$ were used as a check of the mass determination accuracy and experimental resolution. Approximately 100 000 $\Lambda^*(1520)$'s and 150 000 ϕ's were observed in the $\bar{K}^0 K^+ n$ and $\bar{K}^0 K^0 p$ final state, respectively. No evidence for the Θ^+ pentaquark was found in the nK^+ or pK_S invariant mass spectra. Upper limits were set on the production cross section of the reaction $\gamma p \to \bar{K}^0 \Theta^+$ as functions of center-of-mass angle, nK^+ and pK_S masses. Combining the results of the two reactions, the 95% C.L. upper limit on the total cross section for a resonance peaked at 1540 MeV was found to be 0.7 nb. Within most of the available theoretical models, this corresponds to an upper limit on the Θ^+ width, Γ_{Θ^+}, ranging between 0.01 and 7 MeV.

DOI: 10.1103/PhysRevD.74.032001 PACS numbers: 12.39.Mk, 13.60.−r, 13.60.Rj, 14.20.Jn

I. INTRODUCTION

The possible existence of baryon states beyond the usual qqq configuration is of fundamental importance for the understanding of hadronic structure. QCD does not prohibit the existence of exotic states with different configurations such as $qqqq\bar{q}$. In fact, measurements of nucleon structure functions from high energy lepton-nucleon experiments have shown, for example, that ''sea'' quarks ($q\bar{q}$ pairs) contribute significantly to the total momentum of the nucleon. Indeed usual baryons are admixtures of the standard qqq configuration and of $qqqq\bar{q}$, $qqqg$, etc.

In the past, experimental searches focused on pentaquarks, i.e. baryons with a minimal $qqqq\bar{q}$ structure. In 1997, Diakonov and collaborators [1] made definite predictions about the masses and widths of a decuplet of pentaquark states (the so-called ''antidecuplet'') in the framework of a chiral soliton model. The most intriguing aspect of such a multiplet is the presence of three states with exotic quantum numbers or a combination of quantum numbers not allowed for ordinary baryons: the Θ^+ with $S = +1$, the Ξ^{--} and Ξ^+ with $S = -2$. In particular the positive strangeness Θ^+ is not compatible with a qqq state, requiring a minimal quark configuration of the type $uudd\bar{s}$. The widths of the exotic pentaquarks were predicted by

*Current address: University of NH, Durham, NH 03824-3568, USA
†Current address: Old Dominion University, Norfolk, VA 23529, USA
‡Current address: Massachusetts Institute of Technology, Cambridge, MA 02139-4307, USA
§Current address: University of SC, Columbia, SC 29208, USA
‖Current address: Physikalisches Institut der Universität Gießen, 35392 Giessen, Germany
¶Current address: Edinburgh University, Edinburgh EH9 3JZ, United Kingdom
**Current address: University of Massachusetts, Amherst, MA 01003, USA

this model to be very narrow (10–15 MeV) implying that if such states exist they should be directly visible in invariant mass spectra without the need for a more sophisticated partial wave analysis.

The first evidence of a Θ^+ candidate was reported in October 2002 by the LEPS Collaboration, based on the reanalysis of existing data [2]. Several other experimental groups followed [3–12] reporting evidence of a peak in the mass range 1521–1555 MeV. The observation of an isospin partner of the Θ^+ (the Θ^{++}) was recently reported by the STAR Collaboration [13] while the observation of a second pentaquark state, the Ξ^{--} with $dsds\bar{u}$ structure, was reported by the NA49 Collaboration [14]. The first evidence for an anticharmed pentaquark, Θ_c, was reported by the H1 Collaboration [15]. While pentaquark signals observed in each experiment suffered from low statistics, the observations in many different reactions using different probes (photons, electrons, protons, neutrinos) and targets (protons, neutrons, nuclei) supported the pentaquark's existence. On the contrary, subsequent reanalysis of data collected in a different set of experiments [16–29] found no evidence of pentaquarks casting doubts about their existence.

The experimental evidences, both positive and negative, were obtained from data previously collected for other purposes in many reaction channels and in diverse kinematic conditions, thus may involve different production mechanisms. As a result, direct comparisons of the different experiments are very difficult, preventing a definitive conclusion about the pentaquark's existence. A second generation of dedicated experiments [30,31], optimized for the pentaquark search, was undertaken at the Department of Energy's Thomas Jefferson National Accelerator Facility. These experiments covered the few GeV region in photon energy, where most of the positive evidence was reported, and collected at least an order of magnitude more data than used in the previous measurements.

The exclusive reactions $\gamma p \to \bar{K}^0 K^+ n$ and $\gamma p \to \bar{K}^0 K^0 p$ were studied with the CLAS detector [32] with 1.6 to 3.8 GeV energy photons, to look for evidence of the reaction $\gamma p \to \bar{K}^0 \Theta^+$, where the Θ^+ decays into pK^0 or nK^+. The main results for the $\gamma p \to \bar{K}^0 K^+ n$ channel were reported in Ref. [30]. In this paper we discuss in detail the analysis procedure and the results for both decay modes, combining them to give a final consistent result.

For the $\Theta^+ \to nK^+$ decay mode, the measurement of all participating particles allows one to tag the strangeness of the reaction which clearly identifies the exotic nature of the baryon produced in association with the $\bar{K}^0$. For the other possible decay mode, $\Theta^+ \to pK^0$, since a K_S was measured, the strangeness of the pK_S invariant mass system is not defined. Nevertheless, we were motivated to analyze this channel since the majority of the positive results [3,8–12] were reported looking at this decay mode. Moreover the CLAS acceptance for the two reactions is somewhat complementary and the combination of the two channels results in complete kinematic coverage. According to many theoretical predictions, e.g. [33–36], the photon energy range covered by this experiment should be the best to explore since the Θ^+ is expected to have its maximum cross section near the production threshold. Also, in this kinematic region, the CLAS detector provides a mass resolution of few MeV and an accuracy in the mass determination of 1–2 MeV, which is necessary to pin down the mass and width of any narrow peak in the spectrum.

The $\gamma p \to \bar{K}^0 K^+ n$ channel was previously investigated at ELSA by the SAPHIR collaboration [5] in a similar photon energy range, finding positive evidence for a narrow Θ^+ state with $M = 1540$ MeV and FWHM Γ less than 25 MeV. The most recent analysis resulted in a total production cross section of the order of 50 nb. Since this experiment completely overlaps the kinematic regions of the SAPHIR experiment, the new results put those previous findings to a direct test for the first time. Results on pentaquark searches in the exclusive reaction $\gamma p \to \bar{K}^0 K^0 p$ have never been published before.

In the following, some details are given on the experiment (Sec. II) and its analysis (Sec. III). The findings of $\gamma p \to \bar{K}^0 K^+ n$ channel are compared with the SAPHIR experiment in Sec. IV and the systematic checks are discussed in Sec. V. The final results are reported in the last section.

II. THE EXPERIMENT

The measurement was performed using the CLAS detector in Hall B at Jefferson Lab with a bremsstrahlung photon beam produced by a continuous 60 nA electron beam of $E_0 = 4.02$ GeV impinging on a gold foil of thickness 8×10^{-5} radiation lengths. A bremsstrahlung tagging system [37] with a photon energy resolution of 0.1% E_0 was used to tag photons in the energy range from 1.58 GeV (about the $\Theta^+(1540)$ production threshold) to a maximum energy of 3.8 GeV. A cylindrical liquid hydrogen target cell 4 cm in diameter and 40 cm long was used. Outgoing hadrons were detected in the CLAS spectrometer. Momentum information for charged particles was obtained via tracking through three regions of multiwire drift chambers [38] in conjunction with a toroidal magnetic field ($\sim$ 0.5 T) generated by six superconducting coils. The polarity of the field was set to bend the positive particles away from the beam into the acceptance of the detector. Time-of-flight scintillators (TOF) were used for charged hadron identification [39]. The interaction time between the incoming photon and the target was measured by the start counter (ST) [40]. This is made of 24 strips of 2.2 mm thick plastic scintillator surrounding the hydrogen cell with a single-ended PMT-based readout. A time resolution of $\sim$300 ps was achieved. The CLAS momentum resolution, σ_p/p is from 0.5% to 1%, depending on the kinematics. CLAS is

well suited for simultaneous multihadron detection as required by experiments searching for pentaquarks (this experiment required at least 3 hadrons detected). The detector geometrical acceptance for each positive particle in the relevant kinematic region is about 40%. It is somewhat less for low energy negative hadrons, which can be lost at forward angles because their paths are bent toward the beam line and out of the acceptance by the toroidal field. Coincidences between the photon tagger and the CLAS detector triggered the recording of the events. The trigger in CLAS required a coincidence between the TOF and the ST in at least two sectors, in order to select reactions with at least two charged particles in the final state. The collected data sample contains events from several reaction channels in addition to the reactions of interest. Reactions such as $\gamma p \to p\pi^+\pi^-$, $\gamma p \to p\omega$, $\gamma p \to K^+X$, and $\gamma p \to \Sigma^{+(-)}\pi^{-(+)}K^+$ have been used for systematic studies. An integrated luminosity of 70 pb^{-1} was accumulated in 50 days of running in 2004.

III. DATA ANALYSIS

The raw data were passed through the standard CLAS reconstruction software to determine the 4-momenta of detected particles. In this phase of the analysis, corrections were applied to account for the energy loss of charged particles in the target and surrounding materials, misalignments of the drift chambers' position, and uncertainties in the value of the toroidal magnetic field. The energy calibration of the Hall-B tagger system was performed both by a direct measurement of the e^+e^- pairs produced by the incoming photons [41] and by applying an overconstrained kinematic fit to the reaction $\gamma p \to p\pi^+\pi^-$, where all particles in the final state were detected in CLAS [42]. The quality of the calibrations was checked by looking at the mass of known particles as well as their dependence on other kinematic variables (photon energy, detected particle momenta and angles). As an example, Fig. 1 shows the K^+ missing mass spectrum of the reaction $\gamma p \to K^+X$: peaks of known hyperons such as the $\Lambda(1116)$, the $\Sigma^0(1193)$, and related excited states are clearly visible.

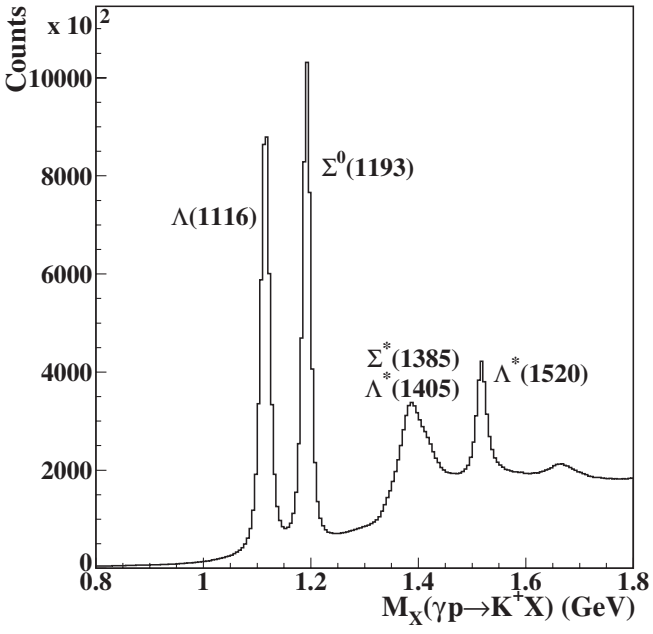

FIG. 1. The K^+ missing mass spectrum for the reaction $\gamma p \to K^+X$. Peaks correspond to ground and excited states of well-known hyperons.

A. Pentaquark analysis strategy

The data set was independently analyzed by three groups that made use of different analysis tools and procedures. This strategy was adopted both to have a corroboration of the analysis results and an estimate of the systematic errors associated with the choice of the analysis procedure. All three analyses agreed on the main conclusions. In the following sections we report in detail the analysis procedure of one group while the comparison of the results from the different groups is discussed in Sec. V C.

B. Reaction identification: $\gamma p \to \bar{K}^0 K^+ n$

The reaction $\gamma p \to \bar{K}^0 K^+ n$ was isolated as follows. The K^+ was directly detected by the spectrometer, while the K_S component of the $\bar{K}^0$ was reconstructed from the invariant mass of its $\pi^+\pi^-$ decay (B.R. $\sim 69\%$). The neutron was then reconstructed from the missing mass of all the detected particles. After its identification, the neutron mass used to calculate other kinematic variables was kept fixed at its nominal PDG value [43]. A $\pm 3\sigma$ cut around the K_S and the neutron peaks was applied to isolate the exclusive reaction. A total of 320 000 events were selected by this procedure. Three background reactions having the same final state as the reaction of interest were clearly identified: $\gamma p \to K^+\Lambda^*(1520)$ with $\Lambda^*(1520) \to n\bar{K}^0$, $\gamma p \to K^+\Sigma^+\pi^-$, and $\gamma p \to K^+\Sigma^-\pi^+$ with $\Sigma^{+(-)} \to n\pi^{+(-)}$. Figure 2 shows the background hyperon peaks: the $\Lambda^*(1520)$ in the K^+ missing mass spectrum and the Σ^+ and Σ^- peaks in the $n\pi^+$ and $n\pi^-$ invariant mass spectra, respectively. We found $M_{\Sigma^+} = 1190 \pm 1$ MeV and $M_{\Sigma^-} = 1198 \pm 1$ MeV, with a measured experimental width $\sigma \sim 3.5$ MeV for both of them. These are in excellent agreement with the world data [43], and are a measure of the quality of the mass determination. Since these states have a much smaller width than the CLAS resolution, their observed widths provide an estimate of the experimental resolution. The reported values are in good agreement with the CLAS resolution estimated from simulations. To remove the contribution of these channels, a $\pm 3\sigma$ cut was applied around the Σ peaks while a ± 24 MeV cut was applied around the $\Lambda^*(1520)$ peak, resulting in a total of 160 000 retained events. The resulting K_S and neutron mass plots are shown in Fig. 3, where the two peaks are

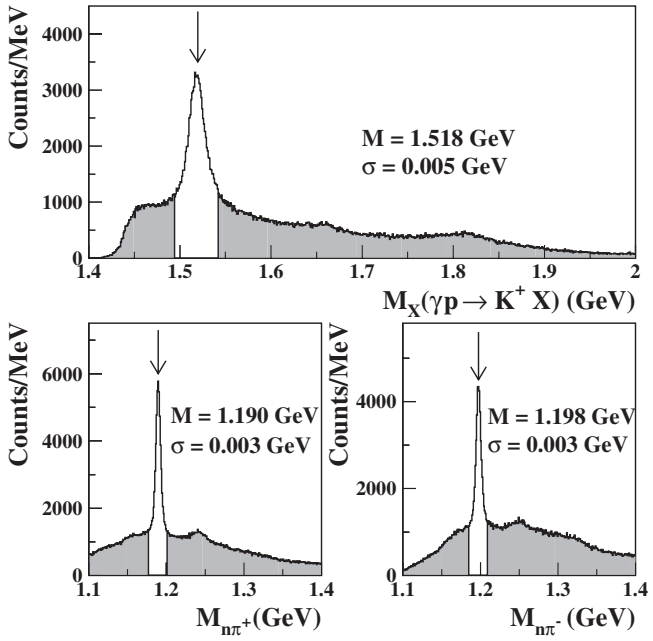

FIG. 2. Hyperon production in the $\gamma p \to \bar{K}^0 K^+ n$ reaction. Top: K^+ missing mass spectrum with the $\Lambda^*(1520)$. Bottom: $n\pi^+$ (left) and $n\pi^-$ (right) invariant mass spectra. The mass position and width of the measured peaks are shown (for the Λ^* the experimental resolution is reported). For comparison the arrows show the world data value for the mass position. The shaded area indicates the retained events.

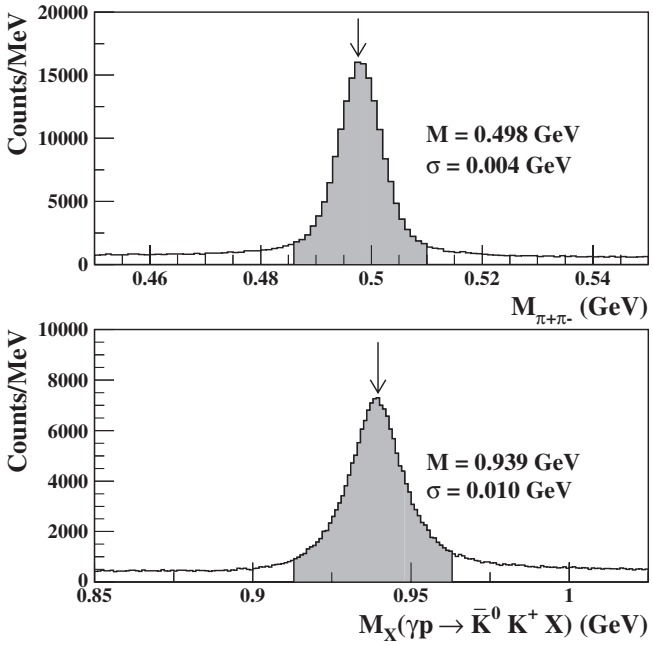

FIG. 3. Mass plots for analysis of the reaction $\gamma p \to \bar{K}^0 K^+ n$. Top: $\pi^+\pi^-$ invariant mass and the $\bar{K}^0$ peak. Bottom: missing mass for the reaction $\gamma p \to \bar{K}^0 K^+ X$ and the neutron peak. The labels show the mass position and width of the measured peaks. For comparison the arrows show the world averages for the mass positions. The shaded area indicates the retained events.

seen above small background levels. The peak positions of the reconstructed K_S and neutron masses were found to be 498 ± 1 MeV and 939 ± 1 MeV respectively.

After all cuts, the resulting nK^+ invariant mass spectrum is shown in Fig. 4. The spectrum is smooth and structureless. In particular no evidence for a peak or an enhancement is observed at masses close to 1540 MeV, where signals associated with the Θ^+ were previously reported. To enhance a possible resonance signal not visible in the integrated spectra, we assumed the two-body reaction $\gamma p \to \bar{K}^0 \Theta^+(1540)$ and selected different $\bar{K}^0$ center-of-mass angle intervals. Figure 5 shows the nK^+ invariant mass spectrum for different $\cos\theta^{\rm CM}_{\bar{K}^0}$ ranges. Monte Carlo studies of the CLAS acceptance for this reaction (see Sec. III E) showed that we could detect events over the entire angular range, in spite of a drop in the efficiency at forward $\bar{K}^0$ angles, $\theta^{\rm CM}_{\bar{K}^0} < 30°$. No structures were found in the spectra when specific angular ranges were selected.

As a demonstration of our sensitivity to baryon resonances, we derived the Λ^* yield. We fit the K^+ missing mass spectrum of Fig. 2 by a Breit-Wigner function convoluted with a Gaussian function to account for the detector resolution, plus a second-order polynomial background. To derive the Λ^* yield, following Ref. [44], we used the Breit-Wigner form:

$$\mathrm{BW} = \frac{M_0 m \Gamma(m)}{(m^2 - M_0^2)^2 + M_0^2 \Gamma(m)^2}, \qquad (1)$$

where

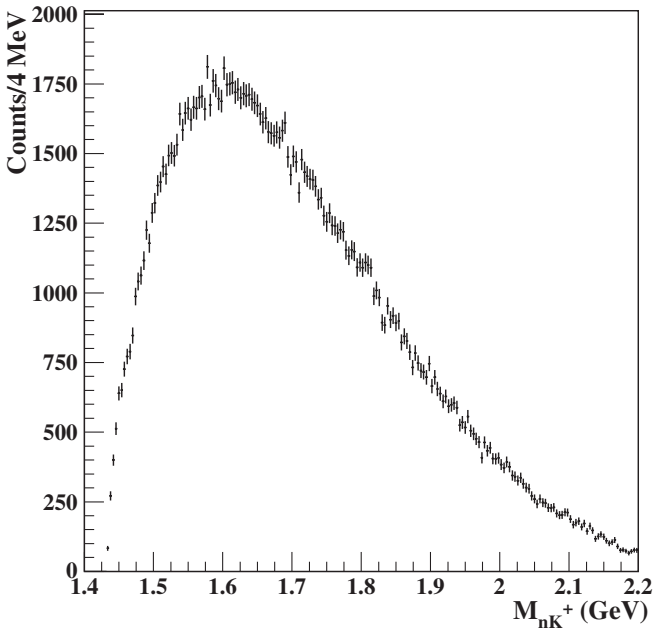

FIG. 4. The nK^+ invariant mass spectrum for the reaction $\gamma p \to \bar{K}^0 K^+ n$ after all cuts, obtained by integrating over all measured photon energies and $\bar{K}^0$ angles.

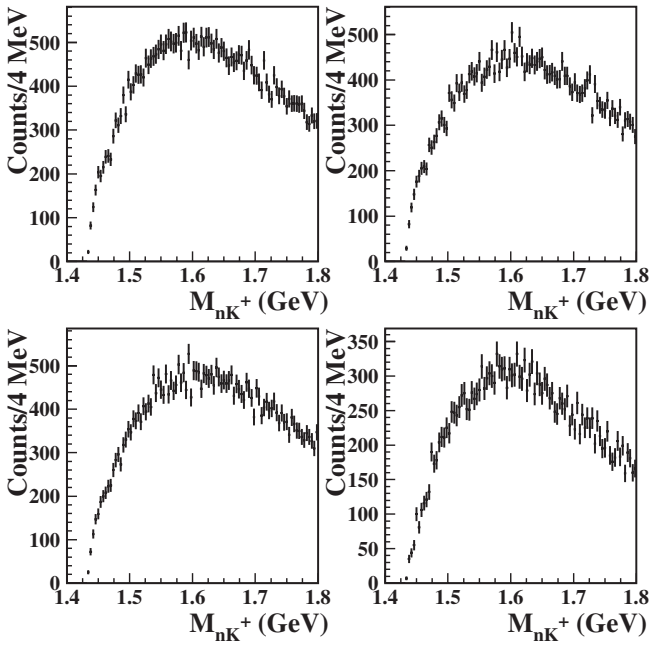

FIG. 5. The nK^+ invariant mass spectrum for the reaction $\gamma p \to \bar{K}^0 K^+ n$ for different $\cos\theta^{\rm CM}_{\bar{K}^0}$ ranges: $\cos\theta^{\rm CM}_{\bar{K}^0} < -0.5$ (top left), $-0.5 < \cos\theta^{\rm CM}_{\bar{K}^0} < 0$ (top right), $0 < \cos\theta^{\rm CM}_{\bar{K}^0} < 0.5$ (bottom left), $\cos\theta^{\rm CM}_{\bar{K}^0} > 0.5$ (bottom right).

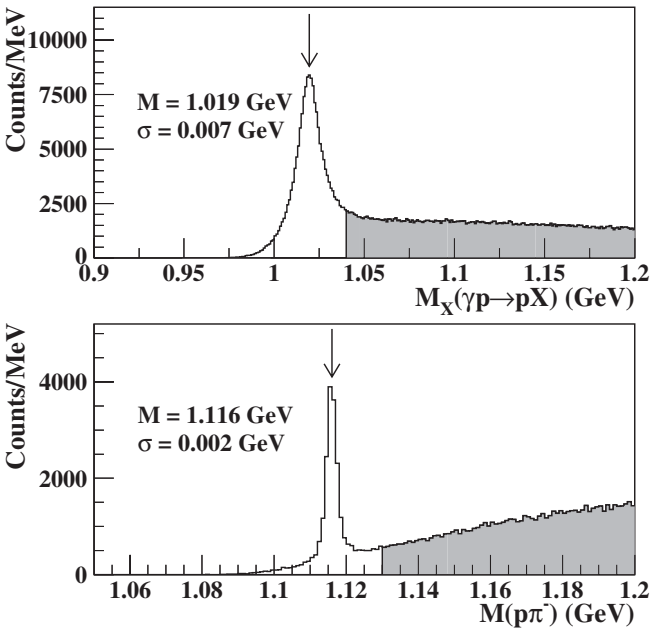

FIG. 6. Background reactions in $\gamma p \to \bar{K}^0 K^0 p$ reaction. Top: proton missing mass spectrum with the ϕ peak. Bottom: $p\pi^-$ invariant mass spectrum; the $\Lambda(1116)$ peak is clearly visible. The mass position and width of the measured peaks are shown. For comparison the arrows show the world data value for the mass position. The shaded area indicates the retained events.

$$\Gamma(m) = \Gamma_0 \left(\frac{Q}{Q_0}\right)^{2l+1},$$

M_0 and Γ_0 are the resonance mass and intrinsic width, Q is the $\bar{K}^0$ momentum in the rest frame of the $n - \bar{K}^0$ system, Q_0 is the same quantity evaluated at the $\Lambda^*(1520)$ peak, and l is the $n - \bar{K}^0$ relative orbital angular momentum ($l = 2$ for the Λ^*). In the fit Γ_0 was fixed to 15.6 MeV [43] while the σ of the Gaussian function was allowed to vary. Integrating the Breit-Wigner line in the mass range 1.45–2.0 GeV we obtained a $\Lambda^*(1520)$ yield of 99 000 ± 10 000. The quoted error is dominated by the systematic uncertainty related to the shape of the Breit-Wigner and the underlying background. The mass position was found to be 1518 ± 2 MeV, in good agreement with world data [43], while the experimental resolution was found to be ~5 MeV, typical for CLAS [32].

C. Reaction identification: $\gamma p \to \bar{K}^0 K^0 p$

To isolate the reaction $\gamma p \to \bar{K}^0 K^0 p$, the proton was detected by the spectrometer and a K_S meson was reconstructed from the invariant mass of its $\pi^+\pi^-$ decay (B.R. ~ 69%). The second neutral kaon was then reconstructed from the missing mass of all the detected particles. A $\pm 3\sigma$ cut around the K_S and the missing kaon peaks was applied to isolate the exclusive reaction. A total of 750 000 events were selected by this procedure. The reaction $\gamma p \to p\phi$ with $\phi \to K_L K_S$ has the same final state as the reaction of interest. The reaction $\gamma p \to \Lambda(1116)\pi^+ K^0 \to p\pi^-\pi^+ K^0$ also contributes to the background. Figure 6 shows the background peaks: the ϕ shows up in the proton missing mass spectrum and the $\Lambda(1116)$ in the $p\pi^-$ invariant mass spectrum. We found $M_\phi = 1019 \pm 1$ MeV and $M_\Lambda = 1116 \pm 1$ MeV, with a measured experimental resolution σ of about 7 MeV and 2 MeV, respectively. The ϕ peak was fitted with a Breit-Wigner ($\Gamma_0 = 4.2$ MeV), convoluted with a Gaussian describing the CLAS resolution, in the same way as was done for the $\Lambda^*(1520)$. The obtained masses are in agreement with world data [43]. To remove the contribution of these channels, only events with a $M_X(\gamma p \to pX) > 1.04$ GeV and $M(p\pi^-) > 1.13$ GeV were retained, resulting in a total of 550 000 events. The two neutral kaon mass spectra after the background rejection are shown in Fig. 7. The two masses were found to be respectively 498 ± 1 MeV and 496 ± 3 MeV.

The selected final state contains two neutral kaons, one detected and one missing, therefore a possible Θ^+ peak can show up in two ways: in the invariant mass spectrum of the pK_S system or in the missing mass spectrum of the detected K_S. Figure 8 shows the two spectra after all cuts: both of them are smooth and structureless. In particular no evidence for a peak or an enhancement is observed at masses close to 1540 MeV, where signals associated with the Θ^+ were previously reported. To enhance a possible resonance signal not visible in the integrated spectra, we assumed the two-body reaction $\gamma p \to \bar{K}^0 \Theta^+(1540)$ and selected different $\bar{K}^0$ center-of-mass angle intervals. The

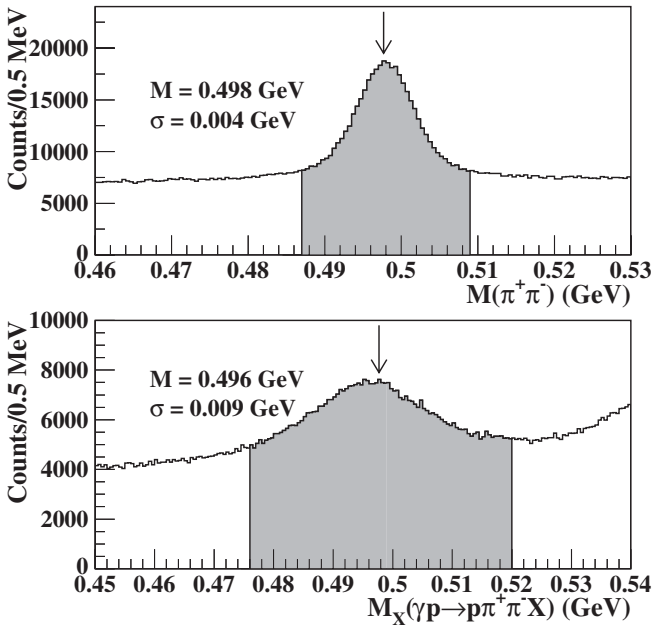

FIG. 7. Mass plots for analysis of the reaction $\gamma p \to \bar{K}^0 K^0 p$. Top: $\pi^+\pi^-$ invariant mass and the K_S peak. Bottom: missing mass for the reaction $\gamma p \to K_S p X$ and the neutral kaon peak. The labels show the mass position and width of the measured peaks. For comparison the arrows show the world averages for the mass positions. The shaded area indicates the retained events.

$\bar{K}^0$ angle was calculated using the reconstructed kinematic variables of the missing kaon in the first case and the measured kinematic variables of the observed kaon in the second case. Figure 9 shows the pK_S invariant mass and the K_S missing mass spectra for forward and backward $\cos\theta^{\rm CM}_{\bar{K}^0}$ ranges separately. When the pK_S system is considered, Monte Carlo studies showed that the CLAS acceptance is maximum at forward $\theta^{\rm CM}_{\bar{K}^0}$ and therefore complementary to what we found for the $\Theta^+ \to nK^+$ decay mode (as seen in Sec. III B). No structures were found in any of the spectra when specific angular ranges were selected.

As shown in Fig. 7 the K_S peak sits over a large background mainly related to multipion production. A cleaner sample is obtained by applying a cut on the K_S decay length: in fact, due to the sizeable K_S mean life ($c\tau \sim 2.68$ cm), its decay vertex ($K_S \to \pi^+\pi^-$) is detached from the primary production vertex ($p\bar{K}^0 K^0$). Taking into account the vertex resolution of the CLAS detector (~ 0.3 cm) and the K_S $c\tau$, we applied a 3 cm decay length cut, obtaining the mass spectra of Fig. 10. Despite the use of a cleaner K_S sample (top panel), no structures are present in the pK_S invariant mass spectrum (bottom panel), confirming the results reported above. The K_S decay length cut improves the signal-to-background ratio for the K_S identification, cleaning the data sample from the multipion contamination. On the other side it reduces the K_S yields by almost a factor five and, due to the strong correlation of the K_S mean life with the kaon momentum, it results in a momentum-dependent cut on the K_S sample, difficult to reproduce by Monte Carlo simulation. This also distorts the pK_S invariant mass spectrum at low values where a

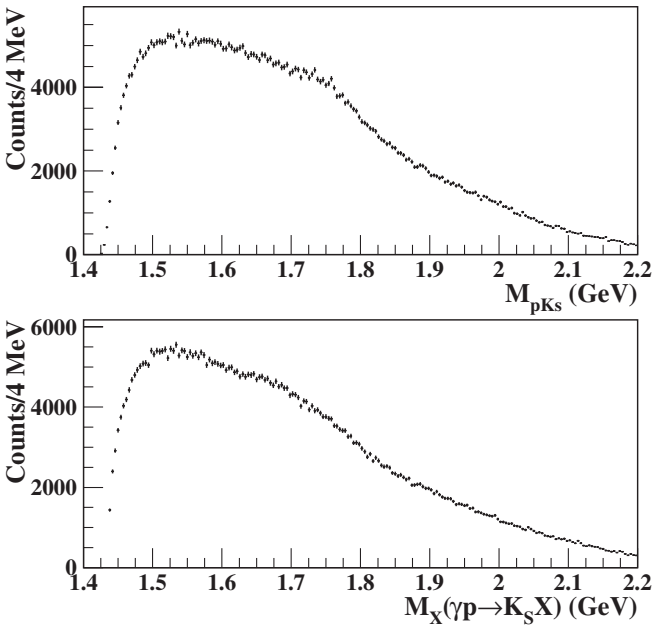

FIG. 8. The pK_S invariant mass (top) and K_S missing mass (bottom) for the reaction $\gamma p \to \bar{K}^0 K^0 p$ after all cuts, obtained by integrating over all measured photon energy and angles. Shoulders corresponding to excited Σ states are visible in both spectra.

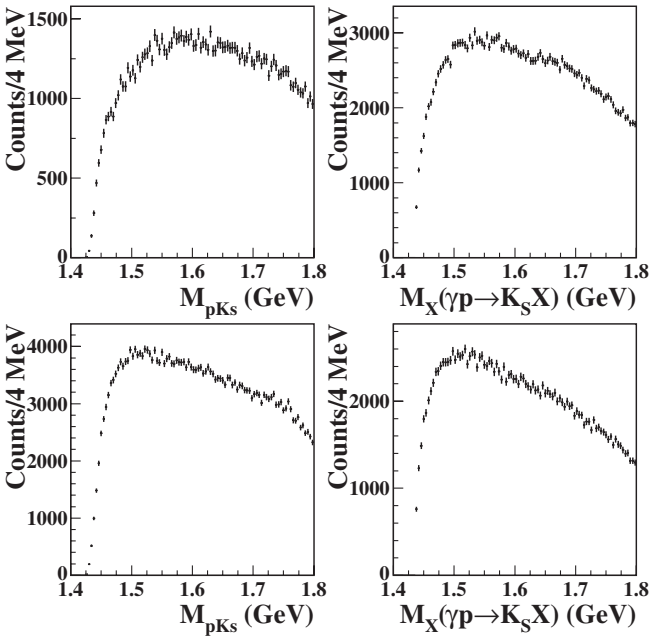

FIG. 9. The pK_S invariant mass (left) and K_S missing mass spectra (right) for the reaction $\gamma p \to \bar{K}^0 K^0 p$ for different angular ranges: $\cos\theta^{\rm CM}_{\bar{K}^0} < 0$ (top), and $\cos\theta^{\rm CM}_{\bar{K}^0} > 0$ (bottom).

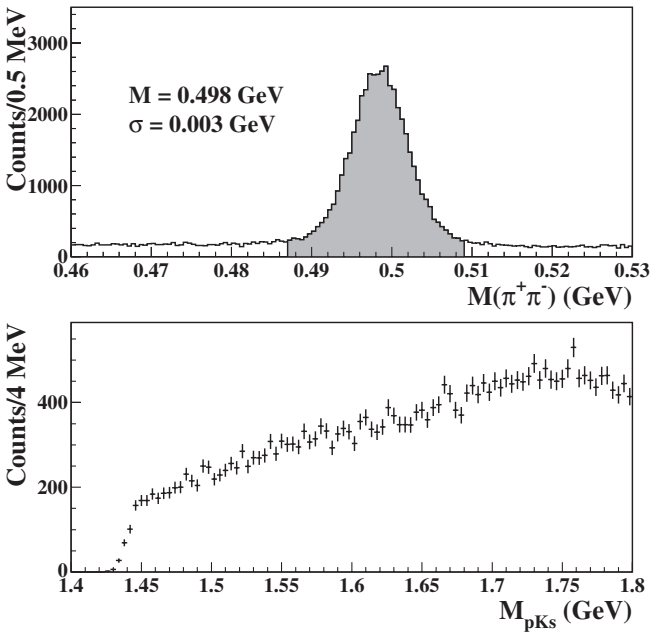

FIG. 10. Effect of the K_S decay length cut on the analysis. Top: $\pi^+\pi^-$ invariant mass and the K_S peak (as in Fig. 7-top). Bottom: pK_S invariant mass (as in Fig. 8-top).

possible resonance is more likely produced. For these reasons, the upper limit for this decay mode are evaluated without the vertex cut.

D. Upper limit on the Θ^+ yields

Since no signal was observed, an upper limit on the Θ^+ yield was extracted and transformed to an upper limit on the production cross section in each reaction channel. In this section we discuss in detail the procedure adopted for the channel $\gamma p \to \bar{K}^0 K^+ n$ and, since the procedure is the same, we summarize the results for the channel $\gamma p \to \bar{K}^0 K^0 p$.

The Θ^+ was assumed to be a narrow peak over a smooth background. The nK^+ invariant mass spectrum was fit to the sum of a Gaussian-shape resonance and a fifth-order polynomial representing the background. The resonance position was varied from 1520 to 1600 MeV in 5 MeV steps while the width was kept fixed assuming the dominance of the experimental resolution over the intrinsic width as suggested from recent analyses of KN scattering data [45].

The Θ^+ width, σ_{Θ^+}, was derived by means of a Monte Carlo simulation. A zero-width resonance was generated and projected over the CLAS detector, applying the same analysis chain used to process the data. A width of σ_{Θ^+} of 3–4 MeV was obtained, which weakly depends on the photon energy and the $\bar{K}^0$ emission angle. To check the consistency of the experimental resolution obtained from the Monte Carlo simulations, the same procedure was applied to the reactions $\gamma p \to K^+\Sigma^+\pi^-$, and $\gamma p \to K^+\Sigma^-\pi^+$ where a direct comparison to the data is possible (see Sec. III B). The width of the two hyperons derived from the simulations was found to be compatible with the measured values. For each value of the Θ^+ mass, the resonance and background yields were extracted using three different fit procedures: (1) a χ^2 fit of the mass distribution binned in 4 MeV channels; (2) a likelihood fit of the unbinned nK^+ spectrum; (3) as in case (1) but with the background function being fit after excluding the signal region defined as $\pm 3\sigma_{\Theta^+}$ around the selected mass value. In all cases the background yield was obtained by integrating the polynomial function over $\pm 3\sigma_{\Theta^+}$ of the selected Θ^+ mass value. In methods (1) and (2) above, the signal yield was obtained as the integral of the resulting Gaussian, while in method (3) it was obtained as the difference between the number of observed events and the background integrated over $\pm 3\sigma_{\Theta^+}$ of the chosen Θ^+ mass value. The same procedure was then repeated subdividing the data into 16 $\cos\theta^{\rm CM}_{\bar{K}^0}$ bins producing binned spectra. The results of the three methods applied to the integrated spectrum are shown in Fig. 11. In general, the signal yields obtained with the three procedures are compatible with zero within 1 or 2 sigma, confirming that no evidence for Θ^+ production is observed in the mass range 1.52–1.6 GeV. The results of the binned χ^2 fits and unbinned likelihood fit are in good agreement with each other showing that the binning effects are small. The measured yields and the background are shown in the top and middle panels of Fig. 12. In general the results of the three methods (χ^2, likelihood, and χ^2 without the Θ^+ mass window) are consistent with each other as expected by the dominance of the background over the signal yield. They were combined by taking the average of the event yields, for both signal and background, in the conservative assumption of totally correlated measurements. The averaged yields were transformed into upper limits of the *true* Θ^+ yield using the Feldman and Cousins approach [46]. This method determines proper confidence-level boundaries for small signals over a background taking into account external constraints (e.g. the *true* yield is constrained to be positive). In addition it decouples the goodness-of-fit confidence level from the confidence-level interval. The resulting upper limit at 95% C.L. is shown in the bottom panel of Fig. 12; it is almost flat with the maximum value around 1545 MeV.

On average, the upper limit at 95% C.L. on the yields is $N_{\Theta^+} \sim 220$. The ratio of the yield of Θ^+ to the $\Lambda^*(1520)$ has also been obtained: $\frac{N_{\Theta^+}}{N_{\Lambda^*(1520)}} \sim 220/99\,000 \sim 0.22\%$ (the two yields are not corrected for the CLAS efficiency). The same procedure was repeated for the $\gamma p \to \bar{K}^0 K^0 p$ channel to derive an upper limit at 95% C.L. on the yield as a function of the pK_S invariant mass and on the differential cross section assuming a Θ^+ mass of 1540 MeV. The upper limit was derived from the pK_S mass spectrum only (the K_S missing mass spectrum was ignored because it is correlated to the pK_S mass spectrum being built from the same

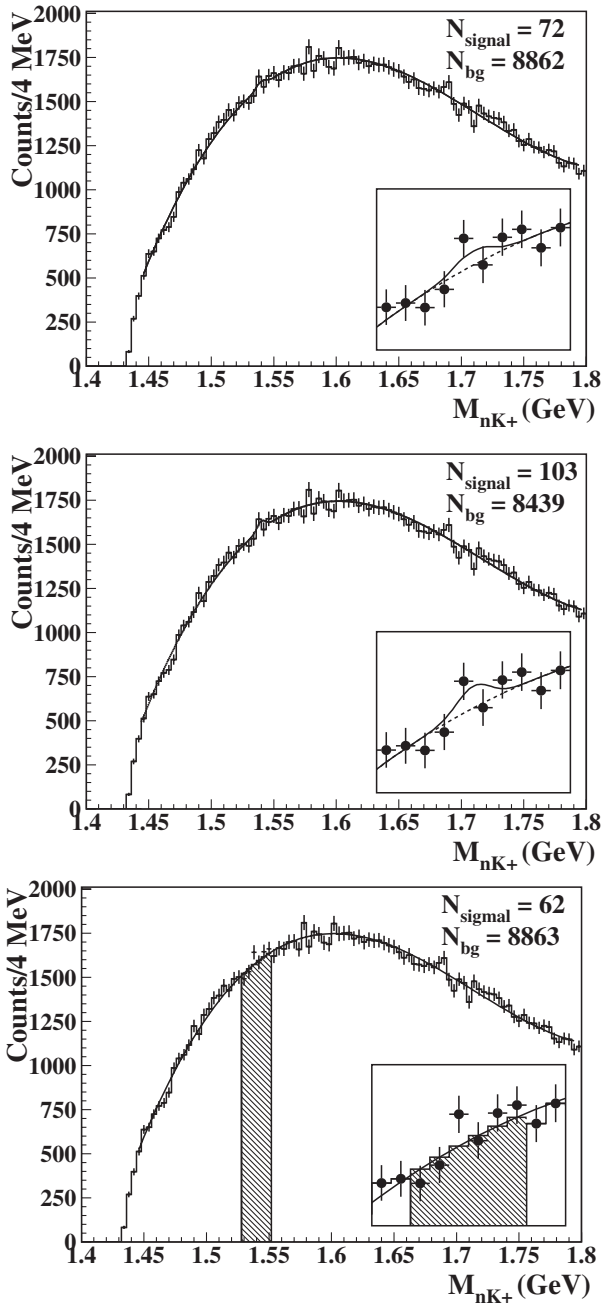

FIG. 11. The nK^+ invariant mass spectrum for the reaction $\gamma p \to \bar{K}^0 K^+ n$ fitted for a Θ^+ mass of 1540 MeV using the three different methods described in the text: from top to bottom the χ^2 fit of the histograms, the likelihood fit of the unbinned events, and the background fit with the exclusion of the Θ^+ mass window (indicated as hatched area). The obtained yields for signal and background are shown on top of each plot. Insets show the zoom of the mass region 1520–1560 MeV.

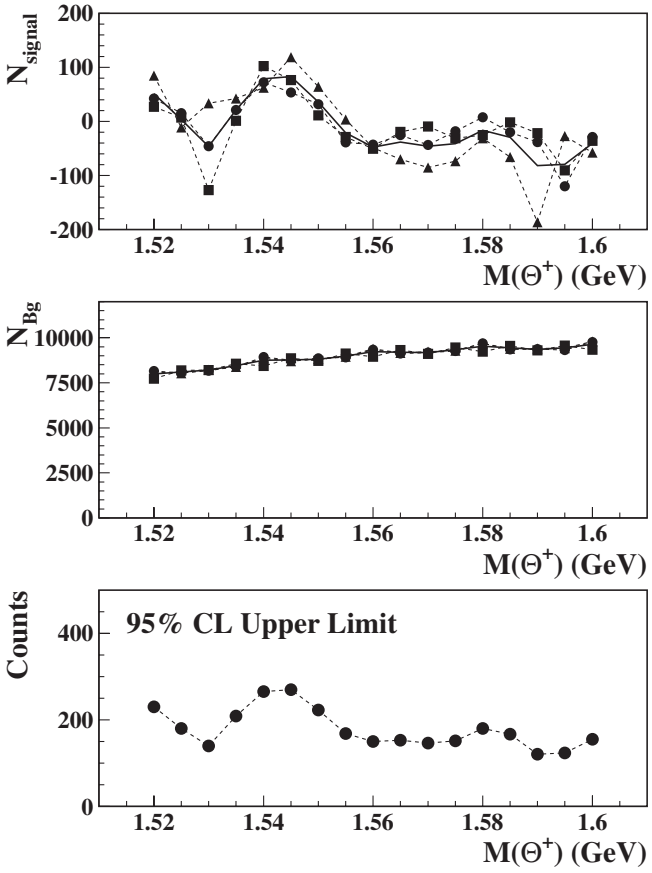

FIG. 12. Signal (top) and background (middle) yields obtained with the three fit procedures for the reaction $\gamma p \to \bar{K}^0 K^+ n$: χ^2 fit of the histograms (circles), likelihood fit of the unbinned events (squares), and background fit with the exclusion of the Θ^+ mass window (triangles). The dashed lines are to guide the eye. The three results were combined together taking the average of the event yields (solid line) and transformed in 95% C.L. upper limit shown in the bottom panel.

event sample). The better CLAS acceptance for the proton and the K_S coming from the Θ^+ decay leads to a complete angular coverage complementary to the $\gamma p \to \bar{K}^0 K^+ n$ channel. The Θ^+ was searched for as a narrow peak by fitting the pK_S mass spectrum with a Gaussian curve with $\sigma_{\Theta^+} \sim 4$ MeV inferred from dedicated Monte Carlo simulations, plus a fifth-order polynomial representing a smooth background. The mass region 1520–1600 MeV was scanned in 5 MeV steps. To derive the yields of a possible resonance and associated background the three fit procedures described for the $\gamma p \to \bar{K}^0 K^+ n$ channel were applied to the integrated spectrum and the $\cos\theta^{CM}_{\bar{K}^0}$-binned spectra for a fixed Θ mass of 1540 MeV. The three results were combined taking the average of the event yields. These were transformed into 95% C.L. upper limits. Figure 13 shows the comparison of the 3 fitted yields as a function of the pK_S invariant mass and the resulting 95% C.L. upper limit.

E. Upper limits on the Θ^+ cross section

The 95% C.L. upper limits on the yield described in the previous section were then transformed into limits on the Θ^+ production cross section according to the following formula:

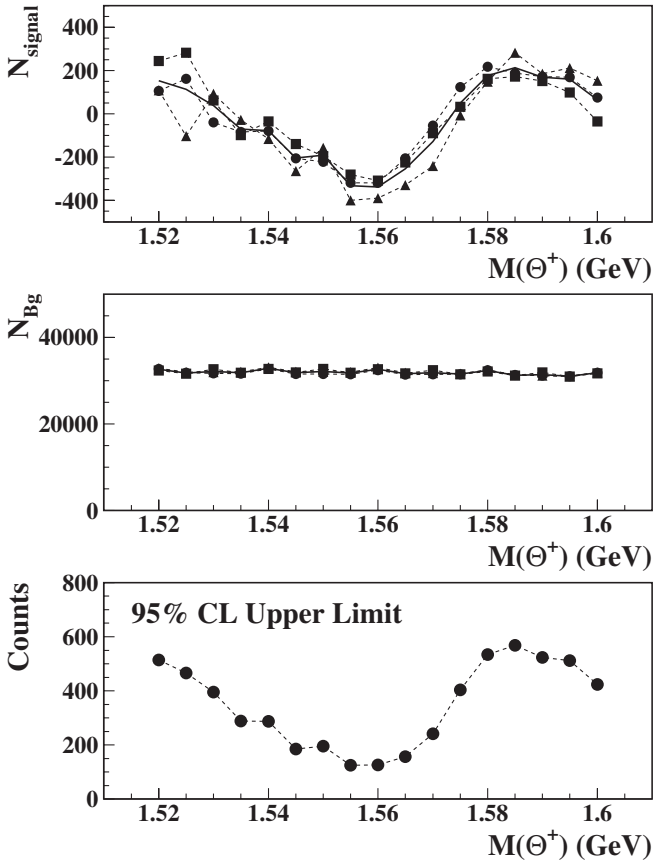

FIG. 13. The same as in Fig. 12 for the $\gamma p \to \bar{K}^0 K^0 p$ channel.

$$\sigma_{nK^+} = \frac{N_{nK^+}}{\mathcal{L}\epsilon_{nK^+} b_{nK^+}} \tag{2}$$

$$\sigma_{pK^0} = \frac{N_{pK^0}}{\mathcal{L}\epsilon_{pK^0} b_{pK^0}} \tag{3}$$

where N is the 95% C.L. limit on the Θ^+ yield, ϵ is the CLAS efficiency, $\mathcal{L}$ is the integrated luminosity, b is the branching ratio for the Θ^+ decay, and subscripts indicate the decay mode of the Θ^+. Each branching ratio is assumed to be 50%. The branching ratios for neutral kaon decay to $K^0 \to K_S \to \pi^+\pi^-$ (50% × 68%) were included in the CLAS efficiency.

The luminosity was obtained as the product of the target density and length, and the incoming photon flux measured during the experiment corrected for data-acquisition dead time. When the Θ^+ mass was varied from 1.5 to 1.6 GeV, the production threshold in beam energy moved from 1.65 to 1.85 GeV. The photon flux used in the cross section estimate was calculated accordingly.

The CLAS detection efficiency was obtained by means of detailed Monte Carlo studies. The reaction $\gamma p \to \bar{K}^0\Theta^+$ and subsequent Θ^+ decay to nK^+ and pK^0 was generated assuming different production mechanisms: t-exchange dominance (the $\bar{K}^0$ mainly produced at forward angles in the center-of-mass system), u-exchange dominance ($\bar{K}^0$ at backward angles), $\cos\theta^{\rm CM}_{\bar{K}^0}$ uniformly distributed, and using the predictions of the model in Ref. [34]. For the t-exchange hypothesis we assumed the same angular distribution as for the reaction $\gamma p \to \Lambda^*(1520)K^+$, which exhibits the typical t-channel forward peaking behavior (approximately an exponential with a slope of -2.5 GeV^{-2}). The u-exchange distribution was generated the same way except that the center-of-mass angles of the $\bar{K}^0$ and Θ^+ were interchanged.

For $\gamma p \to \bar{K}^0\Theta^+$, $\Theta^+ \to K^+ n$, the CLAS overall detection efficiencies obtained with the various production mechanisms vary between 1% for the t-exchange hypothesis to 1.8% for the angular distribution of Ref. [34] when no K^* exchange process is included. As a function of $\theta^{\rm CM}_{\bar{K}^0}$ all the different hypotheses gave a comparable efficiency: almost flat from 180° to 90° (about 2%) and then smoothly dropping at forward angles. For $\gamma p \to \bar{K}^0\Theta^+$, $\Theta^+ \to K^0 p$, the efficiency varied between 1% for the angular distribution of Ref. [34] with no K^* exchange process to 1.8% for the t-channel hypothesis, with an angular dependence complementary to the other channel (smoothly increasing from backward to forward angles). For each branch, the model that yielded the lowest efficiency was chosen for conservatism. The resulting efficiencies are shown in Fig. 14.

The upper limits on the total cross sections as a function of the Θ^+ mass were obtained independently for each decay mode using the model assumptions described above.

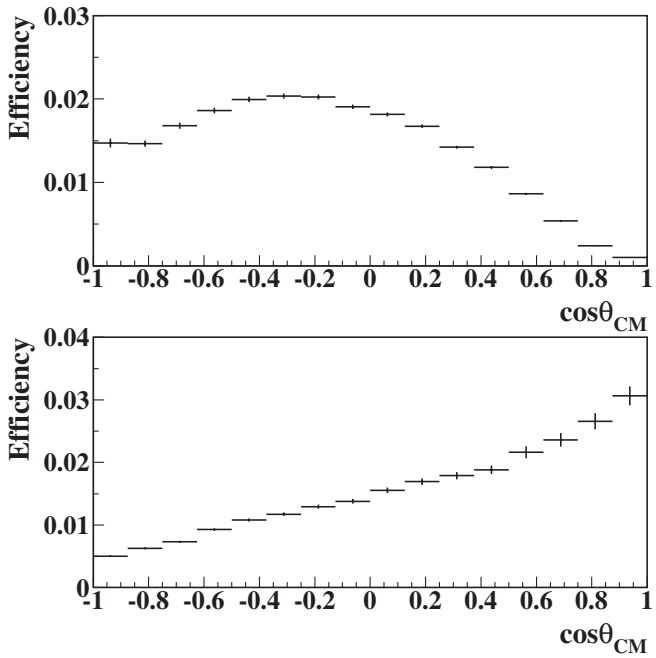

FIG. 14. Binned CLAS efficiency for the reaction $\gamma p \to \bar{K}^0\Theta^+$. Top: $\Theta^+ \to nK^+$ assuming the t-exchange dominance hypothesis; bottom: $\Theta^+ \to pK^0$ assuming the calculation of Ref. [34] with no K^*-exchange. These two correspond to the "worst case scenario" for each decay mode, respectively.

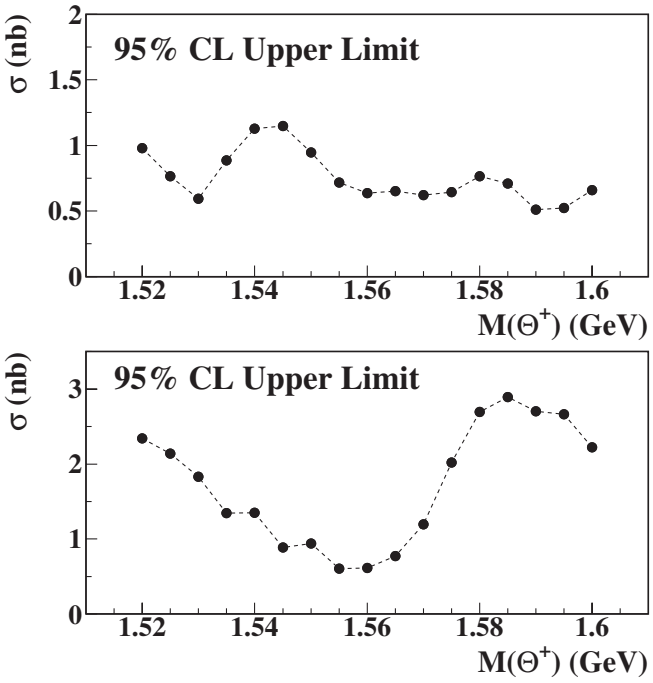

FIG. 15. The 95% Confidence-level upper limit on the total cross section for the reaction $\gamma p \to \bar{K}^0\Theta^+$ with $\Theta^+ \to nK^+$ (top) and $\Theta^+ \to pK^0$ (bottom). The dashed line is to guide the eye.

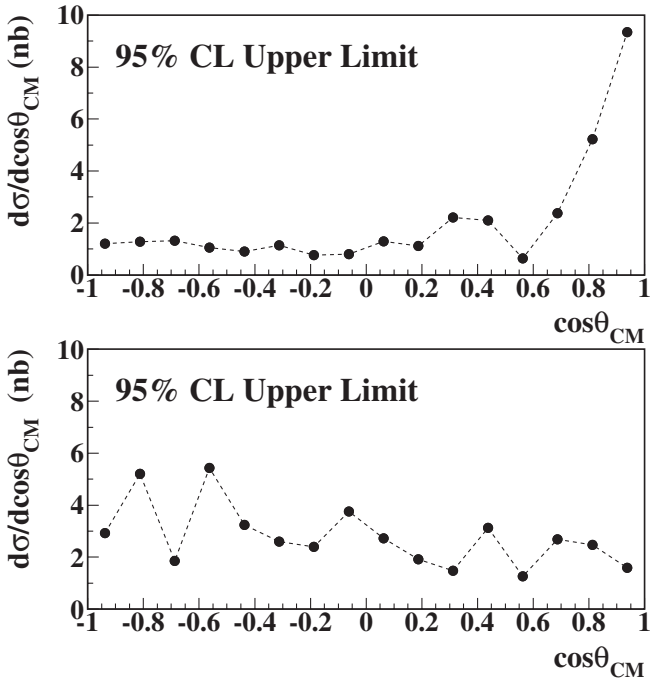

FIG. 16. The 95% confidence-level upper limits on the differential cross section $d\sigma/d\cos\theta^{\rm CM}_{\bar{K}^0}$ for the reaction $\gamma p \to \bar{K}^0\Theta^+(1540)$ obtained from the two decay modes: $\Theta^+(1540) \to nK^+$ (top) and $\Theta^+(1540) \to pK^0$ (bottom). The dashed line is to guide the eye.

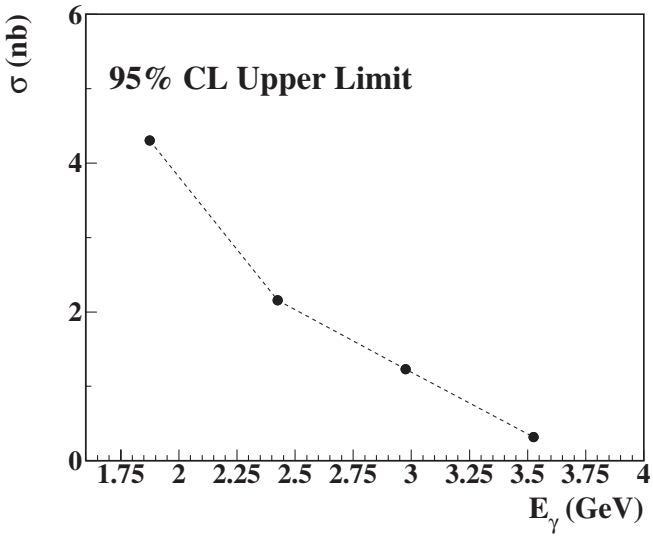

FIG. 17. The 95% confidence-level upper limits on the total cross section as a function of E_γ for the reaction $\gamma p \to \bar{K}^0\Theta^+(1540)$ with $\Theta^+ \to nK^+$. The dashed line is to guide the eye.

The results are shown in Fig. 15. For $\Theta^+ \to nK^+$ a 95% C.L. upper limit of 1.0 nb was found for $M_{\Theta^+} =$ 1540 MeV. The corresponding limit for $\Theta^+ \to pK^0$ was 1.3 nb.

The 95% C.L. upper limit on the $\Theta^+(1540)$ differential cross section $d\sigma/d\cos\theta^{\rm CM}_{\bar{K}^0}$ is shown in Fig. 16, using the same assumption on the production mechanisms as for the evaluation of the upper limit on the total cross section. However, for this quantity no significant difference was found when the other hypotheses were used in the efficiency evaluation. For the nK^+ decay mode the cross section limit remains within 1–2 nb for most of the angular range and rises at forward angle due to the reduced CLAS acceptance. For the pK^0 decay mode, the cross section limit is within 2–5 nb over the entire angular range.

Finally, for the reaction $\gamma p \to \bar{K}^0\Theta^+(1540)$ with $\Theta^+ \to nK^+$, the $\Theta^+(1540)$ total cross section upper limit as a function of the photon energy is shown in Fig. 17; the behavior reflects the CLAS efficiency, which is reduced at low energy near the $\Theta^+(1540)$ production threshold, and then increases with energy, resulting in a better limit for higher energies.

IV. COMPARISON WITH EXISTING DATA

Our result for the reaction $\gamma p \to \bar{K}^0\Theta^+ \to \bar{K}^0K^+n$ is in clear disagreement with the findings of Ref. [5] which reported a Θ^+ signal of 55 events at a mass of 1540 MeV corresponding to an estimated total cross section of 50 nb.

In order to better compare our data with this experiment, the kinematic cuts described in Ref. [5] were applied to the present data. The photon energy was limited to be below 2.6 GeV and a possible forward peaked production of the

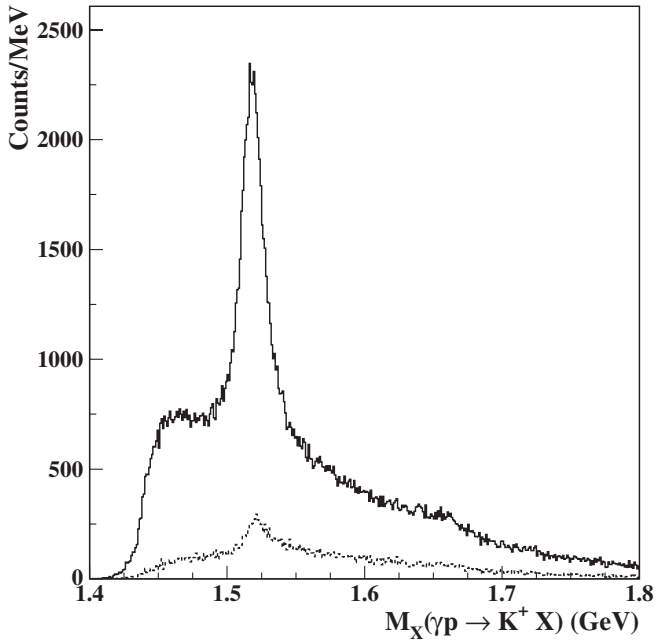

FIG. 18. The CLAS K^+ missing mass showing the $\Lambda^*(1520)$ peak before (solid line) and after (dashed line) cutting on $\cos\theta^{\rm CM}_{\bar{K}^0} > 0.5$.

Θ^+ was selected by applying the angular cut $\cos\theta^{\rm CM}_{\bar{K}^0} > 0.5$. This cut also reduces the hyperon production yield. The effect is shown in Fig. 18 where the missing mass of the K^+ is shown before and after the angular cut: the $\Lambda^*(1520)$ is clearly suppressed. As a result, no hyperon rejection cuts were applied.

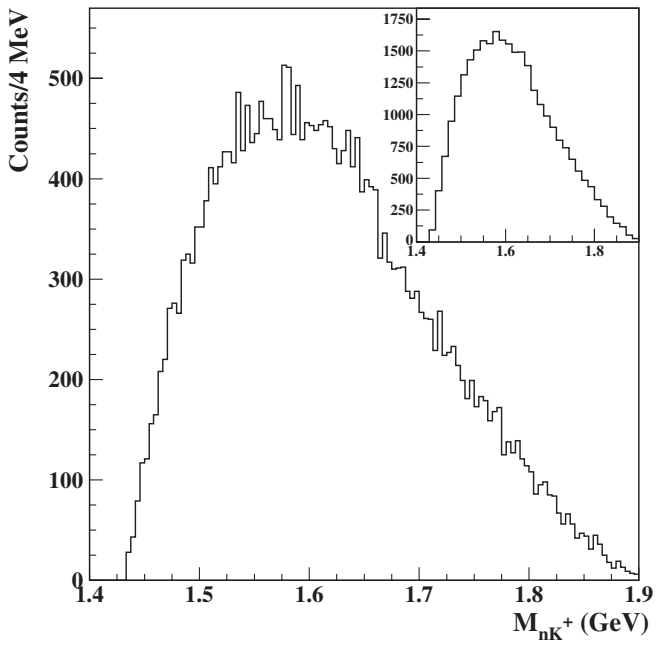

FIG. 19. The CLAS nK^+ invariant mass with all the cuts as in Ref. [5]. The inset show the same spectrum with the binning used by the authors of the same reference.

The $\bar{K}^0$ missing mass spectrum, after all cuts, is shown in Fig. 19 with two different bin sizes reflecting the CLAS and the SAPHIR resolutions. There is no evidence of a Θ^+ peak.

Applying the same procedure described above, we evaluated a 95% confidence level limit on the $\Theta^+(1540)$ yield with SAPHIR selection cuts of 90 events.

To derive the $\Lambda(1520)$ yield, the K^+ missing mass spectrum obtained before the angular cut was fit by a Breit-Wigner function plus a second-order polynomial background, with the same procedure described in Sec. III B, obtaining $(57\,000 \pm 5500)$ $\Lambda^*(1520)$s. This number is to be compared to 630 ± 90 reported by SAPHIR Ref. [5]. The ratio between observed Θ^+ and $\Lambda(1520)$ in this experiment is $\sim$0.16% differing by more than a factor 50 from the value quoted in Ref. [5]. All the yields reported above are not corrected for detector acceptances.

No results were published on the search of the Θ^+ in the exclusive reaction $\gamma p \to \bar{K}^0 K^0 p$ and therefore no comparison is possible for this channel.

V. SYSTEMATIC ERRORS

In the evaluation of the upper limit we have considered the following sources of systematic errors: determination of the mass resolution for the Θ^+ resonance, determination of the signal and background yields from the mass spectra, evaluation of the CLAS efficiency, detector inefficiencies, photon flux normalization, and dependence on the analysis procedure. The first three sources were already included in the quoted upper limit as explained in the following subsections. In particular, the model dependence in evaluating the CLAS efficiency was estimated by comparing the results obtained using different models for the production cross section. The resulting efficiencies differ by a maximum of a factor two. The upper limits were estimated using always the worse case scenario. The remaining sources of systematic uncertainty, summarized in Table I, result in an overall systematic error of $\epsilon = 25\%$ accounted for by multiplying the upper limit by $(1 + \epsilon)$.

In the following, the different contributions to the total systematic error are discussed in more detail.

A. Mass resolution and evaluation of signal and background yields

As discussed in Sec. III D the mass resolution for a narrow resonance was estimated from Monte Carlo simu-

TABLE I. Systematic errors on the upper limit evaluation.

Source	Error (%)
Detector inefficiencies	10
Photon flux normalization	10
Analysis procedure	$<$20

lation; the reliability of simulations in reproducing the CLAS resolution was tested comparing the observed resolution for known narrow resonances and a maximum discrepancy of 20% was found. The resolution for the Θ^+ peak extracted from Monte Carlo was therefore rescaled by a factor 1.2 to account for this.

The comparison of different fitting procedures provides an estimate of the associated systematics. The upper limits were derived combining the results of the three fits, including therefore an estimate of the associated error.

B. Detector inefficiencies and normalization

As a check of the accuracy of the CLAS detector simulations and photon flux normalization, the differential and the total cross section for several known reactions were derived from this data set. Because of the high multiplicity of charged particles in the final state in our data (similar to $\bar{K}^0K^+n$ and $\bar{K}^0K^0p$) and the existence of precise measurements that can be taken as a reference, the reactions $\gamma p \to p\omega$ and $\gamma p \to K^+\Lambda(1116)$ were used as a test of the different ingredients used in our analysis. Moreover, the measurement of different final states of the same reaction, such as $p\pi^+(\pi^-\pi^0)$ and $p\pi^+\pi^-(\pi^0)$ for the ω photoproduction and $K^+p(\pi^-)$ and $K^+p\pi^-$ for the $K^+\Lambda(1116)$ channel, were also used to test the hardware trigger, the photon flux normalization and the procedure to extract the CLAS efficiency. The differential and the total cross sections extracted from this data set agree with each other and with the world data within the experimental error, verifying that the different steps in the analysis are in control at the 15% level.

To directly check our ability to observe the final state involved in the pentaquark decaying into the nK^+ final state, the cross section for the reaction $\gamma p \to K^+\Lambda^*(1520) \to K^+\bar{K}^0n$ was also extracted. As shown above, the $\Lambda^*(1520)$ peak is clearly visible, and the sample of 100 000 Λ^*'s made possible an analysis deriving both the differential and the total cross sections. The $\Lambda^*(1520)$ cross sections we obtained were compared with data from the SAPHIR [47] and NINA [48] collaborations. We are in good agreement with the SAPHIR results but find a much lower cross section than that reported by NINA. The results of all these measurements will be reported elsewhere.

C. Dependence on the analysis procedure

Three independent analyses were conducted both on the reactions of interest for the pentaquark search and on reference reactions as $\gamma p \to \Lambda^*(1520)K^+ \to \bar{K}^0K^+n$. This enabled an evaluation of the systematic errors associated with the analysis procedures and provided a cross check on the results. The three analyses were not totally independent since they all used the same raw data and the same basic corrections to the measured kinematic quantities such as the energy loss. However, they used different particle identification schemes, different detector calibration procedures (for both the tagger system and the CLAS spectrometer), different Monte Carlo simulations to evaluate the CLAS efficiency, and different fit procedures to extract yields.

The $\Lambda^*(1520)$ differential and total cross sections obtained by the three analyses were found to be consistent with each other at the 10% level and agree with the SAPHIR measurement at the same level.

For the reaction $\gamma p \to \bar{K}^0\Theta^+$, all three analyses agreed on the main conclusion: the nK^+ and pK_S spectra are smooth and structureless and, in particular, no signal is observed at 1540 MeV where the Θ^+ pentaquark has been widely reported.

The nK^+ mass spectra for the reaction $\gamma p \to \bar{K}^0K^+n$ obtained by the three analyses are shown in Fig. 20. The difference in the shape of the spectra is mainly related to the different particle identification schemes adopted by the three groups while the small differences in the bin-to-bin fluctuations are due to the different kinematic corrections applied in the analyses. Signal and background yields as a function of the Θ^+ mass resulting from the fit of the three spectra are shown in Fig. 21. The three analyses are consistent at the 10% level on the background estimate while they differ in the event yield evaluation. These discrepancies, reflecting the different choices in the analysis procedures, provide an estimate of the systematic error associated to the extraction of the upper limits.

The same comparison was performed for the $\gamma p \to \bar{K}^0K^0p$ channel with similar results.

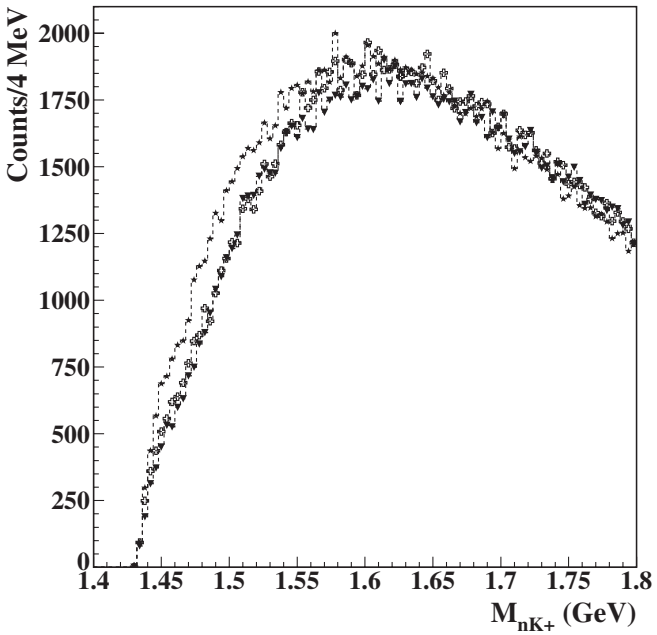

FIG. 20. The final nK^+ spectra for the reaction $\gamma p \to \bar{K}^0K^+n$ obtained by the three independent analyses.

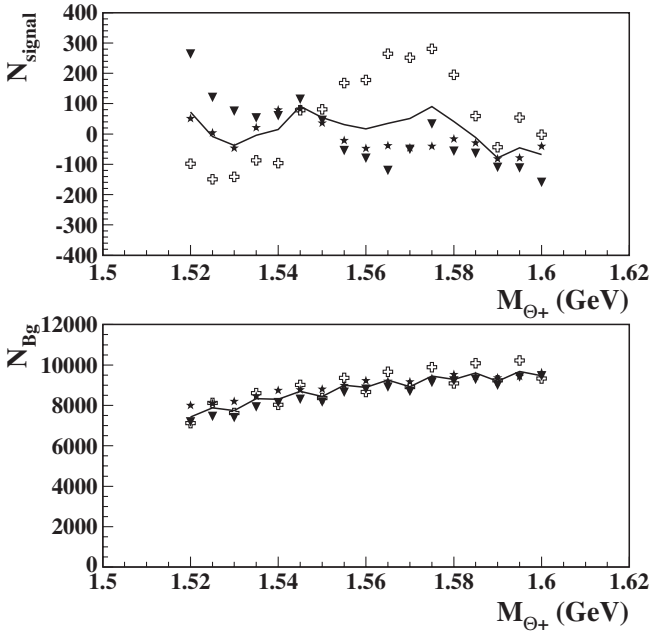

FIG. 21. Signal (top) and background (bottom) yields obtained by the three independent analyses for the reaction $\gamma p \to \bar{K}^0 K^+ n$. Different symbols refer to the different analyses. The solid line shows the average of the three results.

VI. RESULTS

A. Upper limits on the Θ^+ production cross section

The independent analyses were combined, taking the average of the event yields, and transformed into the 95% C.L. upper limit on the yields with the Feldman and Cousins procedure. They were then transformed into the 95% C.L. on the cross section using the CLAS efficiency evaluated in the most conservative scenario. Results are shown in Fig. 22.

For the reaction $\gamma p \to \bar{K}^0 \Theta^+$ with $\Theta^+ \to n K^+$ the upper limit at 95% C.L. on the Θ^+ production cross section varies between 0.5 nb and 1.3 nb as a function of the nK^+ invariant mass with a value of $\sim$0.8 nb at 1540 MeV. For the reaction $\gamma p \to \bar{K}^0 \Theta^+$ with $\Theta^+ \to p K^0$ the upper limit at 95% C.L. on the Θ^+ production cross section varies between 0.5 nb and 2.5 nb as a function of the pK_S invariant mass with a value of $\sim$1.5 nb at 1540 MeV. The results for the two decay modes are similar in value and set stringent upper limits on the models which predict these long-lived pentaquark states.

So far the two reaction channels were independently analyzed. Assuming they result from the two possible decay modes of the Θ^+, they can be combined to give a single upper limit.

As shown in the previous sections, we estimated a signal yield S_i (with $i = 1$ and 2, corresponding to nK^+ and pK^0 branching mode), e.g. the area of a Gaussian of fixed width and fixed mass fit to the mass histogram, and a background yield B_i, e.g. the polynomial background.

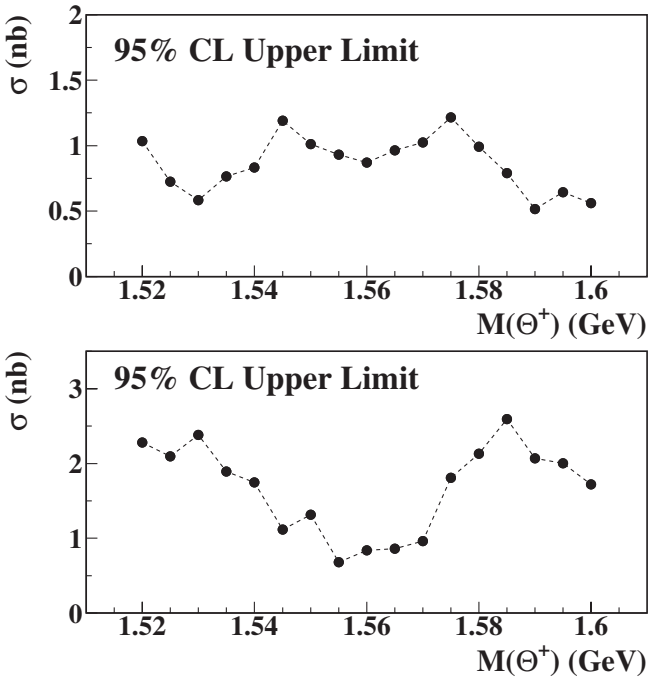

FIG. 22. The 95% C.L. upper limit on the cross section for the reactions $\gamma p \to \bar{K}^0 \Theta^+ \to \bar{K}^0 K^+ n$ (top) and $\gamma p \to \bar{K}^0 \Theta^+ \to \bar{K}^0 K^0 p$ (bottom) derived by the combination of the three analyses. The dashed line is to guide the eye. As explained in the text, the three analyses were largely independent.

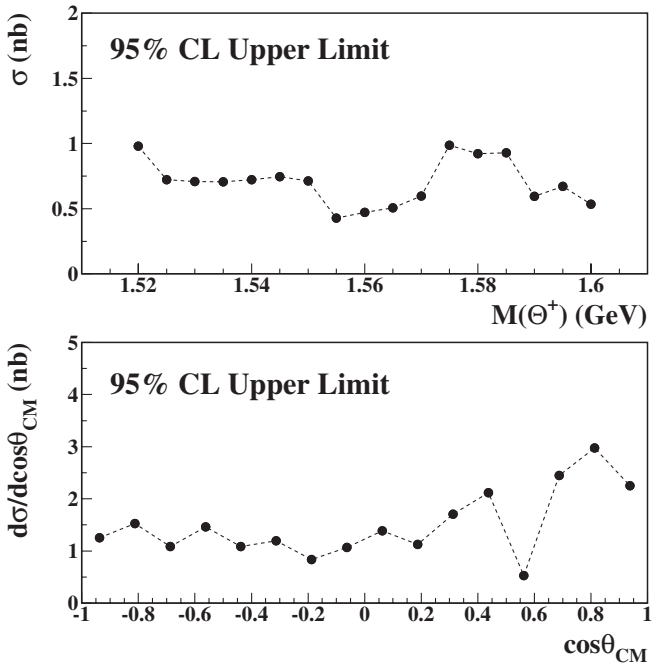

FIG. 23. The 95% C.L. upper limit for the reaction $\gamma p \to \bar{K}^0 \Theta^+$ combining the two channels $\gamma p \to \bar{K}^0 K^+ n$ and $\gamma p \to \bar{K}^0 K^0 p$. The 95% C.L. upper limit on the Θ^+ cross section as a function of Θ^+ mass (top) and the 95% C.L. upper limit on the differential cross section $d\sigma/d\cos\theta^{\rm CM}_{\bar{K}^0}$ for a fixed Θ^+ mass of 1540 MeV. The dashed line is to guide the eye.

These were corrected for the detection efficiency and luminosity to obtain the two corresponding cross sections (σ_i) and associated errors (δ_i):

$$\sigma_i = \frac{S_i}{\mathcal{L}\epsilon_i b_i}, \qquad \delta_i = \frac{\sqrt{S_i + B_i}}{\mathcal{L}\epsilon_i b_i}$$

with b_i the corresponding branching ratios, $\mathcal{L}$ the integrated luminosity and ϵ_i the CLAS detection efficiency.

The cross section for a possible Θ^+ is then built as the weighted average of the two, using the CLAS efficiency evaluated using the five models described in Sec. III E. The dependence on the model assumptions resulted to be within 30%. The largest cross section was obtained in the hypothesis of t-exchange dominance then chosen for conservatism.

The central value divided by its standard deviation constituted the argument of the universal Feldman and Cousins belt graph evaluated for a 95% confidence level for Gaussian statistics. The final results, total cross section as a function of the Θ^+ mass and the differential cross section for MΘ+ = 1540 MeV, are shown in Fig. 23. The 95% C.L. upper limit on the total cross section for a resonance peaked at 1540 MeV was found to be 0.7 nb.

B. Upper limits on Γ_{Θ^+}

The Θ^+ production cross section is directly connected to the Θ^+ width Γ_{Θ^+} (see, for example, Ref. [49]). Therefore upper limits on the cross section imply upper limits on the resonance width. However, this connection depends strongly on the theoretical model, differing by more than an order of magnitude for the available calculations [34–36,49,50]. In Table II, we summarize various theoretical predictions for the total cross section averaged in the energy range 2–4 GeV for different assumptions for parity and spin of the Θ^+ and $\Gamma_{\Theta^+} = 1$ MeV. For example, assuming $J^P = 1/2^+$ our upper limit of 0.7 nb on $\sigma(\gamma p \to \bar{K}^0\Theta^+)$ results in a $\Gamma_{\Theta^+} < 3.2$ MeV within the Regge approach of Ref. [35] and $\Gamma_{\Theta^+} < 0.35$ MeV for the other models. The upper bounds on the Θ^+ width for these models are summarized in Table III.

TABLE II. The Θ^+ total cross section (nb) predicted by different models assuming $\Gamma_{\Theta^+} = 1$ MeV.

J^P	$1/2^+$	$1/2^-$	$3/2^+$	$3/2^-$
[34]	100	0.4		
[35]	0.22	0.1		
[36]	2.0		1.0	3.0
[49]	6.9	3.4	3.2	17.7
[50]	15.0			

TABLE III. Upper limits on the Θ^+ width (MeV) assuming a 95% C.L. of 0.7 nb on the Θ^+ total cross section.

J^P	$1/2^+$	$1/2^-$	$3/2^+$	$3/2^-$
[34]	0.01	1.8		
[35]	3.2	7.0		
[36]	0.35		0.7	0.23
[49]	0.10	0.2	0.2	0.04
[50]	0.05			

VII. CONCLUSIONS

In this paper we report the results of the first Jefferson Lab high statistics and high resolution experiments entirely devoted to the pentaquark search on a nucleon target. The reactions $\gamma p \to \bar{K}^0 K^+ n$ and $\gamma p \to \bar{K}^0 K^0 p$ were studied in search of evidence of the Θ^+ pentaquark in the nK^+ and pK^0 decay channels. The final states were isolated by detecting the K^+ or proton, the K_S via its decay to $\pi^+\pi^-$ and identifying the neutron or the second neutral kaon with the missing mass technique. For the former decay mode, the direct measurement of the K^+ allows the definition of the strangeness of any resonance observed in this final state. A total of 160 000 and 550 000 events were selected for the reaction $\gamma p \to \bar{K}^0 K^+ n$ and $\gamma p \to \bar{K}^0 K^0 p$ respectively, after the exclusion of background reactions. The Θ^+ was searched for as a narrow resonance in the nK^+ and pK_S mass spectra with a width of 3–4 MeV corresponding to the CLAS resolution for these channels in the kinematic region of this experiment. Both mass spectra were found to be smooth and structureless. No evidence for a narrow resonance was found in the mass range 1520–1600 MeV. Combining the results of the two decay modes, we set an upper limit of 0.7 nb (95% confidence level) on the total production cross section for the reaction $\gamma p \to \bar{K}^0\Theta^+(1540)$. This contradicts the results previously reported for a resonance in the reaction channel $\gamma p \to \bar{K}^0 K^+ n$.

The accuracy in the mass determination was found to be 1–2 MeV from the comparison of the measured masses of known particles with world data. The quality of the data and the analysis procedures were tested by deriving the differential and the total cross section for some known reactions and obtaining an agreement within the experimental errors with existing measurements. The same conclusions were found by several independent analyses, giving confidence in our final results.

Because of the loose hardware trigger of the experiment, the same data set was analyzed to study the reactions $\gamma p \to \bar{K}^*\Theta^+$ and $\gamma p \to K^-\Theta^{++}$ [51]. These findings, together with the results coming from other pentaquark search experiments at Jefferson Lab, could clear up the debate about the existence of the pentaquark.

ACKNOWLEDGMENTS

We would like to acknowledge the outstanding efforts of the staff of the Accelerator and the Physics Divisions at Jefferson Lab that made this experiment possible. This work was supported in part by the Italian Istituto

Nazionale di Fisica Nucleare, the French Centre National de la Recherche Scientifique and Commissariat à l'Energie Atomique, the U.S. Department of Energy and National Science Foundation, and the Korea Science and Engineering Foundation. The Southeastern Universities Research Association (SURA) operates the Thomas Jefferson National Accelerator Facility for the United States Department of Energy under Contract No. DE-AC05-84ER40150.

[1] D. Diakonov, V. Petrov, and M. Polyakov, Z. Phys. A **359**, 305 (1997).
[2] T. Nakano *et al.* (LEPS Collaboration), Phys. Rev. Lett. **91**, 012002 (2003).
[3] V. V. Barmin *et al.* (DIANA Collaboration), Phys. At. Nucl. **66**, 1715 (2003).
[4] S. Stepanyan *et al.* (CLAS Collaboration), Phys. Rev. Lett. **91**, 252001 (2003).
[5] J. Barth *et al.* (SAPHIR Collaboration), Phys. Lett. B **572**, 127 (2003); M. Ostrick, Prog. Part. Nucl. Phys. **55**, 337 (2005).
[6] V. Kubarovsky *et al.* (CLAS Collaboration), Phys. Rev. Lett. **92**, 032001 (2004).
[7] A. E. Asratyan, A. G. Dolgolenko, and M. A. Kubantsev, Phys. At. Nucl. **67**, 682 (2004).
[8] A. Airapetian *et al.* (HERMES Collaboration), Phys. Lett. B **585**, 213 (2004).
[9] S. Chekanov *et al.* (ZEUS Collaboration), Phys. Lett. B **591**, 7 (2004).
[10] A. Aleev *et al.* (SVD Collaboration), Phys. At. Nucl. **68**, 974 (2005); hep-ex/0509033.
[11] M. Abdel-Bary *et al.* (COSY-TOF Collaboration), Phys. Lett. B **595**, 127 (2004).
[12] P. Z. Aslanyan, V. N. Emelyanenko, and G. G. Rikhkvitzkaya, Nucl. Phys. **A755**, 375 (2005).
[13] H. Huang *et al.* (STAR Collaboration), Int. J. Mod. Phys. A **21**, 825 (2006).
[14] C. Alt *et al.* (NA49 Collaboration), Phys. Rev. Lett. **92**, 042003 (2004).
[15] A. Aktas *et al.* (H1 Collaboration), Phys. Lett. B **588**, 17 (2004).
[16] S. Schael *et al.* (ALEPH Collaboration), Phys. Lett. B **599**, 1 (2004).
[17] B. Aubert *et al.* (*BABAR* Collaboration), hep-ex/0408064.
[18] K. Abe *et al.* (Belle Collaboration), hep-ex/0411005.
[19] J. Z. Bai *et al.* (BES Collaboration), Phys. Rev. D **70**, 012004 (2004).
[20] I. V. Gorelov (CDF Collaboration), hep-ex/0408025; D. O. Litvintsev (CDF Collaboration), Nucl. Phys. B, Proc. Suppl. **142**, 374 (2005).
[21] K. Stenson (FOCUS Collaboration), Int. J. Mod. Phys. A **20**, 3745 (2005).
[22] I. Abt *et al.* (HERA-B Collaboration), Phys. Rev. Lett. **93**, 212003 (2004); K. T. Knopfle, M. Zavertyaev, and T. Zivko (HERA-B Collaboration), J. Phys. G **30**, S1363 (2004).
[23] M. J. Longo *et al.* (HyperCP Collaboration), Phys. Rev. D **70**, 111101(R) (2004).
[24] J. Napolitano, J. Cummings, and M. Witkowski, hep-ex/0412031.
[25] S. R. Armstrong, Nucl. Phys. B, Proc. Suppl. **142**, 364 (2005).
[26] C. Pinkenburg (PHENIX Collaboration), J. Phys. G **30**, S1201 (2004).
[27] Y. M. Antipov *et al.* (SPHINX Collaboration), Eur. Phys. J. A **21**, 455 (2004).
[28] M. I. Adamovich *et al.* (WA89 Collaboration), Phys. Rev. C **72**, 055201 (2005).
[29] E. S. Ageev *et al.* (COMPASS Collaboration), Eur. Phys. J. C **41**, 469 (2005).
[30] M. Battaglieri *et al.* (CLAS Collaboration), Phys. Rev. Lett. **96**, 042001 (2006).
[31] B. McKinnon *et al.* (CLAS Collaboration), Phys. Rev. Lett. **96**, 212001 (2006).
[32] B. Mecking *et al.*, Nucl. Instrum. Methods Phys. Res., Sect. A **503**, 513 (2003).
[33] T. Mart, Phys. Rev. C **71**, 022202(R) (2005).
[34] Y. Oh, H. Kim, and S. H. Lee, Phys. Rev. D **69**, 014009 (2004); Nucl. Phys. A **745**, 129 (2004); Y. Oh, K. Nakayama, and T.-S. H. Lee, Phys. Rep. **423**, 49 (2006).
[35] H. Kwee, M. Guidal, M. V. Polyakov, and M. Vanderhaeghen, Phys. Rev. D **72**, 054012 (2005).
[36] S. Nam *et al.*, Phys. Lett. B **633**, 483 (2006).
[37] D. I. Sober *et al.*, Nucl. Instrum. Methods Phys. Res., Sect. A **440**, 263 (2000).
[38] M. D. Mestayer *et al.*, Nucl. Instrum. Methods Phys. Res., Sect. A **449**, 81 (2000).
[39] E. S. Smith *et al.*, Nucl. Instrum. Methods Phys. Res., Sect. A **432**, 265 (1999).
[40] Y. G. Sharabian *et al.*, Nucl. Instrum. Methods Phys. Res., Sect. A **556**, 246 (2006).
[41] S. Stepanyan *et al.*, CLAS Report No. 2005-012.
[42] M. Williams *et al.*, CLAS Report No. 2004-017.
[43] S. Eidelman *et al.*, Phys. Lett. B **592**, 1 (2004).
[44] J. D. Jackson, Nuovo Cimento **34**, 1644 (1964).
[45] R. A. Arndt, I. I. Strakovsky, and R. L. Workman, Phys. Rev. C **68**, 042201(R) (2003); R. N. Cahn and G. H. Trilling, Phys. Rev. D **69**, 011501(R) (2004); J. Haidenbauer and G. Krein, Phys. Rev. C **68**, 052201(R) (2003); W. R. Gibbs, Phys. Rev. C **70**, 045208 (2004); A. Sibirtsev *et al.*, Phys. Lett. B **599**, 230 (2004).
[46] G. J. Feldman and R. D. Cousins, Phys. Rev. D **57**, 3873 (1998).
[47] E. Klempt *et al.*, *Proceedings of Baryons '98 Conference, Bonn, 1998* (World Scientific, Singapore, 1998).
[48] D. Barber *et al.*, Z. Phys. C **7**, 17 (1980).
[49] W. Roberts, Phys. Rev. C **70**, 065201 (2004).
[50] C. M. Ko and W. Liu, nucl-th/0410068.
[51] V. Kubarovsky *et al.* (CLAS Collaboration), hep-ex/0605001.